Environmental Science and Pollution Research (2019) 26:8768–8778
https://doi.org/10.1007/s11356-019-04394-w

RESEARCH ARTICLE

Synergistic effect and degradation mechanism on Fe-Ni/CNTs for removal of 2,4-dichlorophenol in aqueous solution

Yufeng Sun[1,2] · Zongtang Liu[2] · Zhenghao Fei[2] · Changshun Li[1] · Yuan Chun[1] · Aimin Zhang[1]

Received: 19 October 2018 / Accepted: 25 January 2019 / Published online: 2 February 2019

Abstract

Fe-Ni bimetallic nanoparticles supported on CNTs (Fe-Ni/CNTs) were synthesized, characterized, and applied for removal of 2,4-dichlorophenol (2,4-DCP) in aqueous solution. The removal performance was enhanced drastically on Fe-Ni/CNTs with respect to monometallic Fe/CNTs. The synergistic effect between Fe-Ni nanoparticles and CNTs has been studied in detail. The research results indicated that the doping of Ni played an important role in promoting the catalytic degradation of 2,4-DCP. And the presence of CNTs not only could effectively reduce the aggregation of nanoparticles but also facilitate the mass transfer of 2,4-DCP and the formation of active atomic hydrogen during the catalytic process. In addition, the removal kinetics of 2,4-DCP by Fe-Ni/CNTs were in agreement with a pseudo-first-order model, and the rate constants were dependent on a number of factors including the initial concentration of 2,4-DCP, the dosage of Fe-Ni/CNTs, pH value of the solution, and doping amount of Ni. The degradation mechanism involved the adsorption by CNTs and catalytic reduction by Fe under the stimulating of Ni, and the preferred dechlorination followed the order of para-Cl > ortho-Cl. The study confirmed that Fe-Ni/CNTs had a potential to be a promising catalytic material for removal of chlorophenol and had a great prospect for practical application.

Keywords Supported Fe-Ni nanoparticles · CNTs · 2,4-dichlorophenol · Degradation · Synergistic effect

Introduction

As an important member in the family of chlorinated phenols, 2,4-dichlorophenol (2,4-DCP) is a kind of significant industrial raw materials, which is extensively employed in the manufacture of wood preservatives, pesticides, fungicides, and herbicides (Sun et al. 2013; Nasser and Mingelgrin 2014; Fang et al. 2018). However, it has also been regarded as priority pollutants by the United States Environmental Protection Agency owing to its high toxicity, carcinogenicity, recalcitrance, and bioaccumulation (Contreras et al. 2003; Pulido Melian et al. 2013). The widespread use of 2,4-DCP engenders discharge of 2,4-DCP into water and soil environments, resulting in great health threat to humans and ecosystems over a long period of time (Witonska et al. 2014; Li et al. 2015). It is thus urgent to develop effective treatment methods for the removal of 2,4-DCP prior to disposal.

Nanoscale zero-valent iron (nZVI) has been suggested as a promising candidate for removal of a variety of chlorinated organics with a high reactivity and relatively low economic and environmental costs (Song and Carraway 2005; Cheng et al. 2007; Tsang et al. 2009; Shih et al. 2011; Zhang et al. 2012). It is widely accepted that the removal pathways of reductive dechlorination involve either electron transfer or reaction with H_2 generated from nZVI corrosion (Wei et al. 2006; Gao et al. 2016). However, unlike chlorinated aliphatics, its reaction rate is generally slow due to chlorinated aromatics, which may result in the accumulation of toxic byproducts from partial dechlorination and introduction of new contaminants in the environment (Zhou et al. 2010; Li et al. 2013). Furthermore, the formation of iron oxide or hydroxide over the surface of nZVI is inevitable (Zhang et al. 2009; Nagpal et al. 2010), which considerably decreases the

Responsible editor: Philippe Garrigues

Electronic supplementary material The online version of this article (https://doi.org/10.1007/s11356-019-04394-w) contains supplementary material, which is available to authorized users.

✉ Aimin Zhang
zhangamchem@163.com

[1] Key Laboratory of Mesoscopic Chemistry of MOE, School of Chemistry and Chemical Engineering, Nanjing University, Nanjing 210023, People's Republic of China

[2] School of Chemistry and Environmental Engineering, Yancheng Teachers University, Yancheng 224002, People's Republic of China

effective use of nZVI. Therefore, the nZVI system has been further advanced through coating the second metal such as Pd or Ni on the substrate-metal surface to form bimetallic nanoparticles (Wei et al. 2006; Cheng et al. 2010; O'Carroll et al. 2013; Sahu et al. 2018). Ni is a preferred doping metal in the nZVI system because of its availability and reasonable cost compared with noble metal (Cheng et al. 2010; Li et al. 2017). The H_2 produced from nZVI corrosion may be further activated by doping catalytic metal and utilized to accelerate the dechlorination process (Gao et al. 2016; Zhou et al. 2016). Our previous study has also proved that Ni possesses excellent catalytic hydrogenation performance, and the hydrogen can be dissociated to active atomic hydrogen over Ni surface (Sun et al. 2016). Overall, Ni with excellent adsorption-dissociation capacity for hydrogen can change the customary electron-transfer mechanism to catalytic hydrodechlorination mechanism, which brings about a rapid, effective, and complete dechlorination process (Fang et al. 2011; Wu et al. 2014; Liu et al. 2015). Nevertheless, freshly prepared Fe-based nanoparticles are apt to aggregate due to the high surface energies and intrinsic magnetic interactions (Li et al. 2017), leading to adverse effects on its reactivity. Hence, how to improve the dispersion and prevent aggregation has become a new challenge for Fe-based nanoparticles application.

To address this issue, various supports including montmorillonite, bentonite, vermiculite, silica, and resin have been developed to immobilize nanoparticles for eliminating the pollutants in aqueous solution (Chen et al. 2009; Su et al. 2011; Wu et al. 2014; Doong et al. 2015; Zhou et al. 2016; Mishra et al. 2017). As a novel nanostructured carbon material, carbon nanotubes (CNTs) have attracted great research interest due to their unique characteristics such as large specific surface area, high mechanical strength, high adsorption capacity for hydrogen, and the exhibition of their extensive applications as adsorbent and catalyst support (Kim et al. 2005; Kragulj et al. 2015; Chaudhary et al. 2017). Compared with other support materials, CNTs also have excellent electrical property, which is advantageous for electron transfer (Sun et al. 2016). We expect to improve the degradation performance of Fe-based bimetallic nanoparticles for pollutants in the presence of CNTs. To our knowledge, no study has been reported to remove 2,4-DCP in aqueous solution over the Fe-Ni bimetallic nanoparticles supported on CNTs (Fe-Ni/CNTs). More complete and systematic studies of the catalytic removal of 2,4-DCP using Fe-Ni/CNTs and especially an understanding of promoting action of Ni in the presence of CNTs are needed.

Herein, we prepared Fe-Ni/CNTs by the liquid-phase chemical reduction method for the catalytic removal of 2,4-DCP with higher concentration in aqueous solution. In this study, we mainly focused on the following: (1) the synthesis and characterization of Fe-Ni/CNTs, (2) a number of important parameters that affect the hydrodechlorination of 2,4-DCP, (3) the synergistic effect between Fe-Ni nanoparticles and CNTs, and (4) the removal kinetics and possible degradation mechanism.

Material and methods

Chemical

Ferrous sulfate heptahydrate ($FeSO_4·7H_2O$), nickel chloride hexahydrate ($NiCl_2·6H_2O$), sodium borohydride ($NaBH_4$), sodium hydroxide (NaOH), hydrochloric acid (HCl), nitric acid (HNO_3), and ethyl alcohol absolute (C_2H_6O) were purchased from Sinopharm Chemical Reagent Co., Ltd. (China). 2,4-Dichlorophenol (2,4-DCP), 2-chlorophenol (2-CP), 4-chlorophenol (4-CP), and phenol (P) were purchased from Aladdin Industrial Co., Ltd. (China). All chemicals were of analytical grade, except otherwise noted, and did not undergo any further purification. HPLC grade methanol was obtained from Tedia Company Inc. (USA). The 2,4-DCP stock solution was prepared by dissolving 2,4-DCP in distilled water and stored at 4 °C before use.

Catalyst preparation

Raw multi-walled CNTs were supplied by Chengdu Organic Chemicals Co., Ltd. of the Chinese Academy of Science (China). Initially, they were pretreated by concentrated nitric acid at 100 °C or 120 °C as described in our previous study (Sun et al. 2016) and then used as support material. Fe-Ni nanoparticles supported on CNTs (Fe-Ni/CNTs) were prepared under a nitrogen atmosphere by the liquid-phase chemical reduction method (Zhou et al. 2014) and the detailed procedures were described as follows. Firstly, a certain amount of $FeSO_4·7H_2O$ was dissolved in 100 mL distilled water with the addition of 0.50 g of pretreated CNTs, followed by mechanical stirring at 250 rpm for 1 h for complete admixture. Subsequently, 50 mL of 0.5 mol/L $NaBH_4$ as a reducing agent was added dropwise into the suspension and stirred continuously for another 2 h. The prepared material was filtered and quickly washed three times with distilled water and ethyl alcohol absolute, successively. Afterward, a certain amount of $NiCl_2·6H_2O$ was absolutely dissolved in 100 mL distilled water, and the above freshly prepared material was quickly added in the solution. The mixture was sequentially stirred at 250 rpm for 1 h. After that, the solid was separated from the suspension by vacuum filtration and quickly rinsed seriatim with distilled water and ethyl alcohol absolute. The theoretical mass ratio of the sum of Fe and Ni and CNTs in the prepared Fe-Ni/CNTs was 1:1 and Fe and Ni was 4:1. For comparison, Ni supported on CNTs (Ni/CNTs) and Fe supported on CNTs (Fe/CNTs) were synthesized by the same as above procedures, and the mass ratio of Ni:CNTs and

Fe:CNTs was 1:1. The preparation of Fe-Ni nanoparticles was performed under identical conditions but without CNTs, and the mass ratio of Fe and Ni was 4:1. Furthermore, Fe-Ni/AC was also prepared with the same method using active carbon as support. All the resultant samples were dried at 60 °C under vacuum overnight and stored under nitrogen atmosphere prior to the experiment.

Catalyst characterization

Scanning electron microscopy (SEM) images were acquired using S-4800 scanning electron microscopy equipped with energy dispersive spectrometer operating at 5 kV. Transmission electron microscope (TEM) observations were carried out with JEOL-JEM-2000 transmission electron microscope at an accelerating voltage of 200 kV. Powder X-ray diffraction (XRD) measurements were performed on Philips X'pert Pro X-ray diffractometer with Cu Kα radiation at an accelerating voltage of 40 kV and an emission current of 40 mA. The BET surface areas were determined by N_2 adsorption-desorption isotherms at −196 °C using Micromeritics ASAP 2020 apparatus. Raman spectra were recorded on a Horiba Jobin Yvon LabRam Aramis Raman spectrometer at a laser excitation wavelength of 532 nm. X-ray photoelectron spectroscopy (XPS) was made with a PHI5000 VersaProbe electron spectrometer. All the binding energies were referenced to C_{1s} at 284.6 eV.

Catalytic removal experiment

Under a nitrogen atmosphere, a certain amount of samples including CNTs, Ni/CNTs, Fe/CNTs, Fe-Ni/CNTs, Fe-Ni, and Fe-Ni/AC were added, respectively, to a 250 mL four-necked flask containing 100 mL of 2,4-DCP solution and agitated at 250 rpm for 4 h. Samples were withdrawn from the flask with glass syringes at selected time intervals and passed through 0.22 μm filter membranes and further transferred to a 2.0 mL high-performance liquid chromatography (HPLC) vial. The effect of various parameters, such as initial concentration of 2,4-DCP (100, 200, 300, 400, and 500 mg/L), dosage of Fe-Ni/CNTs (0.75, 1.5, 3.0, 4.5, and 6.0 g/L), pH values of solution (3, 4, 5, 6, 7, 9, and 11), and doping amount of Ni (0, 10, 16, 20, 24, and 30% of Ni/Fe ratio) on the catalytic removal of 2,4-DCP in aqueous solution by Fe-Ni/CNTs, was also evaluated. Moreover, the degradation performance of 2,4-DCP on Fe-Ni/CNTs pretreated at 100 °C was also tested. The liquid phase catalytic hydrodechlorination of 2,4-DCP on Ni/CNTs, Fe/CNTs, and CNTs was performed in a four-necked flask containing 2,4-DCP solution under a hydrogen atmosphere. All experiments were carried out in triplicate. The quantitative concentrations of target pollutant (2,4-DCP), dechlorination intermediates (2-CP and 4-CP), and final product (P) were measured with a HPLC (Dionex UltiMate 3000, USA) equipped with a UV-vis detector at a wavelength of 280 nm and a C18 column (4.6 mm × 150 mm, 5.0 μm). The mobile phase of methanol/water mixture in the proportion 70/30 (*V*/*V*) was used at a flow rate of 1.0 mL/min. The size of the sample loop was 20 μL.

Results and discussion

Characterization

The morphology of CNTs, Fe-Ni, Fe/CNTs, Fe-Ni/CNTs, and Fe-Ni/CNTs-r (after reaction with 2,4-DCP in aqueous solution) was characterized by SEM and the results were shown in Fig. 1. The SEM image as presented in Fig. 1a confirmed the integrated tubular structure of CNTs, and the surface of CNTs was smooth in appearance. The unsupported Fe-Ni existed as prominent chain-like aggregates because of their high surface energies and magnetic interactions (Fang et al. 2011; Li et al. 2017) as shown in Fig.1b. In contrast, for the sample Fe/CNTs, it was observed obviously that the supported nanoparticles were dispersed onto the external surface of CNTs as displayed in Fig. 1c. For the sample Fe-Ni/CNTs, lots of nanoparticles were same supported on the surface of CNTs and remained well-dispersed as shown in Fig. 1d. Evidently, the aggregation of nanoparticles expectedly decreased after supporting by CNTs, indicating that the CNTs played an important role in dispersing and stabilizing the supported nanoparticles. However, in the case of Fe-Ni/CNTs-r as shown in Fig. 1e, the morphology of the sample changed significantly and the additional products with needle-like structure were newly formed on the surface of the sample. From the TEM images as depicted in Fig. 1f, it could be seen clearly that the spherical nanoparticles were well-dispersed onto the CNTs surface and the size ranged from 20 to 80 nm.

The XRD patterns of CNTs, Fe-Ni, Fe/CNTs, Fe-Ni/CNTs, Fe-Ni-r, and Fe-Ni/CNTs-r were illustrated in Fig. 2. The support CNTs had characteristic peaks of 26.0° and 43.0° (Song et al. 2010; Sun et al. 2016) and the relative peak intensity apparently decreased due to loading. The distinct peak at the 2θ= 44.7° confirmed the existence of Fe^0 in freshly prepared Fe-Ni, Fe/CNTs, and Fe-Ni/CNTs (Weng et al. 2014; He et al. 2018). Nevertheless, the typical peak of Fe^0 became too weak to be visible in XRD patterns of Fe-Ni-r and Fe-Ni/CNTs-r. New additional peaks appeared distinctly at 27.0°, 35.4°, 36.5°, 46.8°, and 60.5° suggested the formation of Fe_2O_3, Fe_3O_4, and FeOOH which perhaps corresponded to the needle-like products (Kanel et al. 2005; Weng et al. 2014; Xu et al. 2014). The localized elemental information of Fe-Ni/CNTs and Fe-Ni/CNTs-r was determined by EDS analysis

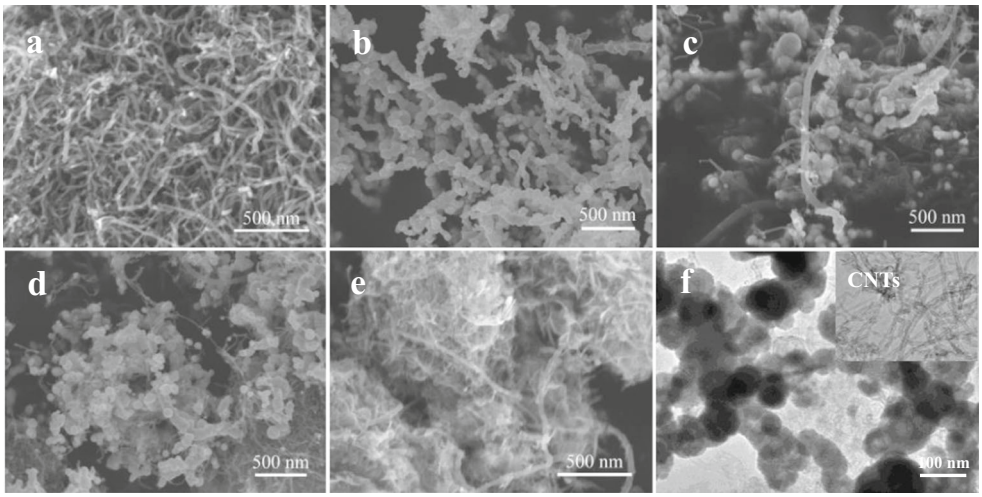

Fig. 1 SEM images of CNTs (**a**), Fe-Ni (**b**), Fe/CNTs (**c**), Fe-Ni/CNTs (**d**), Fe-Ni/CNTs-r (**e**), and TEM images of CNTs and Fe-Ni/CNTs (**f**)

as revealed in Fig. S1 and the specific relative weight percentage of C, O, Fe, and Ni was listed in Table 1. It was obvious that the Fe content in Fe-Ni/CNTs-r decreased from 34.19 to 13.09% whereas the O content increased from 16.19 to 44.99%. The phenomenon could be explained by the corrosion of Fe as a reductant to form iron ions, iron oxide, hydroxide, and oxygen-containing groups on the surface of the catalyst during reaction process (Kanel et al. 2005; Nagpal et al. 2010; Zhou et al. 2014).

The measured BET specific surface areas of CNTs, Fe-Ni, Fe/CNTs, and Fe-Ni/CNTs were 223.0, 31.9, 200.2, and 122.2 m^2/g, respectively. It could be seen that the specific surface areas of Fe/CNTs and Fe-Ni/CNTs increased greatly compared with unsupported Fe-Ni due to Fe or Fe-Ni nanoparticles dispersed onto CNTs with large specific surface area (Wu et al. 2014). However, the specific surface area of Fe-Ni/CNTs was apparently smaller than Fe/CNTs, indicating that bimetallic component might have a distinct influence on the structure of CNTs.

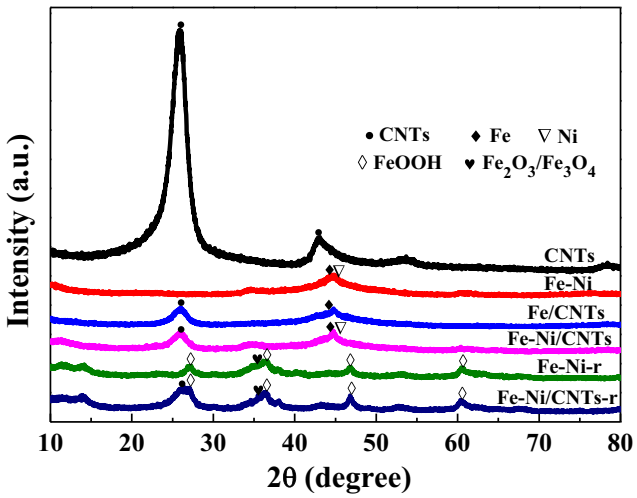

Fig. 2 XRD patterns of CNTs, Fe-Ni, Fe/CNTs, Fe-Ni/CNTs, Fe-Ni-r, and Fe-Ni/CNTs-r

Performance of catalytic removal for 2,4-DCP in aqueous solution

The removal performance of CNTs, Ni/CNTs, Fe/CNTs, Fe-Ni/CNTs, Fe-Ni, and Fe-Ni/AC for 2,4-DCP in aqueous solution was represented in Fig. 3. It could be seen that 22.9% of 2,4-DCP was removed by CNTs alone. The equilibrium was reached in less than 5 min and kept unchanged during 240 min. Obviously, the support CNTs had rapid adsorption capacity for 2,4-DCP in aqueous solution. The sample Ni/CNTs had about 24.2% of 2,4-DCP removal efficiency, which was close to the adsorption value of CNTs. It illustrated that the single component Ni supported on CNTs under this condition almost had no catalytic activity. For the sample Fe/CNTs, it was noticed that the removal efficiency of 2,4-DCP was also similar to that of CNTs at initial 90 min and afterward it began to increase gradually and arrived at 40.1% after 240 min. It was evidently attributed to the catalytic degradation action of Fe^0. However, for the sample Fe-Ni/CNTs, the removal efficiency of 2,4-DCP was drastically increased and reached to 91.7%. Accordingly, we also investigated the catalytic degradation performance of unsupported Fe-Ni sample, which possessed impressive removal efficiency of 62.7% as depicted in Fig. 3. Although the total amount of bimetallic component was larger than that of Fe-Ni/CNTs in the experiment, this result well revealed the promoting action of Ni doping for catalytic degradation. The compared sample Fe-Ni/AC using active carbon as support exhibited the removal efficiency of about 75.2% under the same conditions in spite

Table 1 Relative weight percentage of C, O, Fe, and Ni in Fe-Ni/CNTs and Fe-Ni/CNTs-r by EDS analysis

Sample	C (%)	O (%)	Fe (%)	Ni (%)
Fe-Ni/CNTs	40.41	16.19	34.19	9.21
Fe-Ni/CNTs-r	36.69	44.99	13.09	5.23

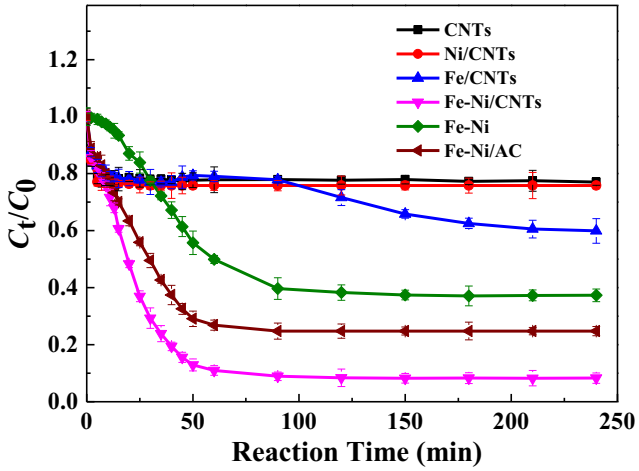

Fig. 3 Removal of 2,4-DCP by various materials (Conditions C_0, 300 mg/L; dosage of CNTs, 1.5 g/L; dosage of Ni/CNTs, 3.0 g/L; dosage of Fe/CNTs, 3.0 g/L; dosage of Fe-Ni/CNTs, 3.0 g/L; dosage of Fe-Ni, 3.0 g/L; dosage of Fe-Ni/AC, 3.0 g/L; Ni doping amount, 20%; temperature, 30 °C)

of the larger specific surface area. Therefore, the 2,4-DCP removal efficiency of 91.7% on the sample Fe-Ni/CNTs was the jointly promoting result of Fe-Ni nanoparticles and CNTs.

Parameters affecting the catalytic removal for 2,4-DCP

Effect of initial concentration

The effect of initial concentration on the removal of 2,4-DCP by Fe-Ni/CNTs was studied. As shown in Fig. 4, Fe-Ni/CNTs exhibited excellent catalytic removal performance for 2,4-DCP when the initial concentration was less than 300 mg/L. More than 90% of 2,4-DCP was removed after 60 min, even it reached 99.1% at the concentration of 100 mg/L. The removal capacity improved tremendously compared with the result of

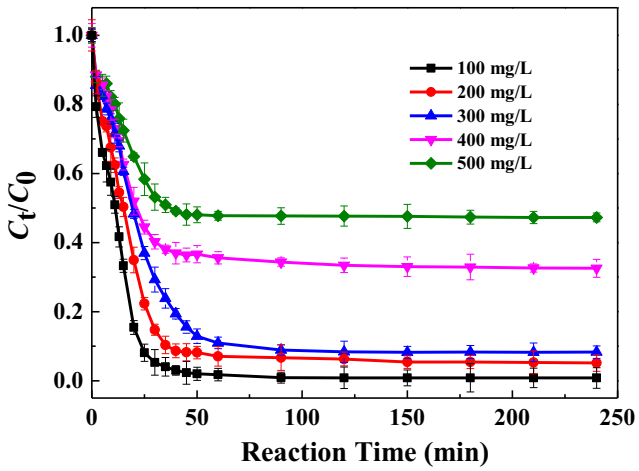

Fig. 4 Effect of initial concentration on the removal of 2,4-DCP by Fe-Ni/CNTs (Conditions dosage of Fe-Ni/CNTs, 3.0 g/L; Ni doping amount, 20%; temperature, 30 °C)

the 2,4-DCP removal using MWNT-Pd/Fe at the initial concentration of 20 mg/L (Xu et al. 2012). The removal efficiency decreased distinctly when the initial concentration of 2,4-DCP further increased to more than 400 mg/L. It was only 52.2% at a 2,4-DCP concentration of 500 mg/L within the same contact time. Furthermore, the removal of 2,4-DCP by Fe-Ni/CNTs could be satisfactorily fitted by the pseudo-first-order kinetic model expression with a correlation coefficient (R^2) greater than 0.978 as elaborated in Table 2. It was obvious that the k_{obs} decreased with the increase of initial 2,4-DCP concentration. Generally, the degradation of 2,4-DCP on composite materials was a heterogeneous reaction involving adsorption and the subsequent surface reaction. Increasing the initial concentration of 2,4-DCP would lead to competitive adsorption among the 2,4-DCP molecules due to the limited adsorption capacity and available active sites on Fe-Ni/CNTs at a fixed dosage (Chen et al. 2011; Weng et al. 2014).

Effect of Fe-Ni/CNTs dosage

The effect of Fe-Ni/CNTs dosage on the removal of 2,4-DCP was presented in Fig. 5. The removal efficiency of 2,4-DCP increased significantly from 24.2 to 91.7% when the Fe-Ni/CNTs dosage increased from 0.75 to 3.0 g/L. When the dosage was up to 4.5 g/L, the removal efficiency of 2,4-DCP

Table 2 Estimated regression parameters of pseudo-first-order kinetic model for 2,4-DCP

Influencing factors		R^2	k_{obs} (1/h)
Initial concentration mg/L	100	0.978	5.500
	200	0.980	3.706
	300	0.988	2.410
	400	0.982	1.751
	500	0.982	1.147
Fe-Ni/CNTs dosage g/L	0.75	0.980	0.602
	1.5	0.982	1.469
	3.0	0.988	2.410
	4.5	0.986	7.090
	6.0	0.982	10.868
Solution pH	3	0.989	0.703
	4	0.991	1.277
	5	0.993	1.747
	6	0.982	3.834
	7	0.980	1.033
	9	0.989	0.230
	11	0.987	0.162
Ni doping amount %	10	0.990	0.908
	16	0.985	1.467
	20	0.988	2.410
	24	0.984	3.310
	30	0.981	1.491

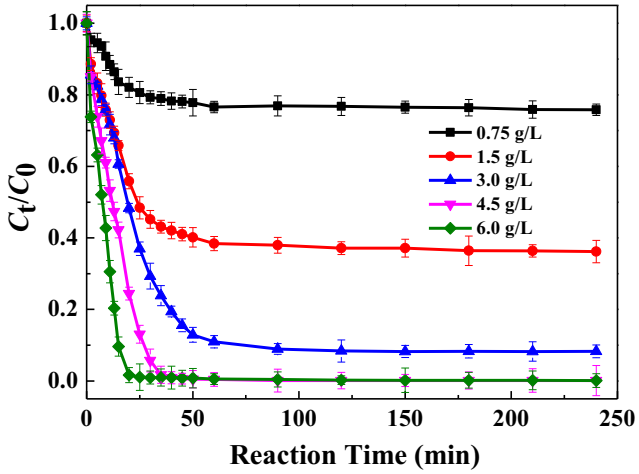

Fig. 5 Effect of Fe-Ni/CNTs dosage on the removal of 2,4-DCP (Conditions C_0, 300 mg/L; Ni doping amount, 20%; temperature, 30 °C)

reached maximum and the almost entire removal of 2,4-DCP was observed. Further enhancement of Fe-Ni/CNTs dosage had no obvious effect. The enhanced removal of 2,4-DCP would be owing to that an increase in the amount of Fe-Ni/CNTs led to an increase in available active sites for adsorption and reduction of 2,4-DCP (Chen et al. 2011; Liu et al. 2013). Based on Table 2, linear relationships existed between $\ln(C_t/C_0)$ versus t for experiments with different dosage and the k_{obs} increased as Fe-Ni/CNTs dosage increased.

Effect of solution pH

The effect of solution pH on the removal of 2,4-DCP by Fe-Ni/CNTs was evaluated. It was found that the reactivity of Fe-Ni/CNTs towards 2,4-DCP removal was strongly pH-dependent as shown in Fig. 6. When the solution pH values increased from 3 to 11, the removal efficiency of 2,4-DCP first increased from 53.0 to 93.6% and then decreased to 21.9% within 240 min. It was noticeable that a maximum level of removal efficiency was observed at pH value of 6, suggesting that optimal 2,4-DCP dechlorination occurred under weak acidic condition. A reasonable explanation was that sufficient hydrogen was obtained through the corrosion of iron in aqueous solution, and the active hydrogen involved in the dechlorination of 2,4-DCP was produced (Zhou et al. 2016). It was crucial because the dechlorination process was catalytic hydrogenation and active atomic hydrogen acted as the predominant reducing agent (Liu et al. 2015). However, under alkaline conditions, the formed surface passivating layers of metal oxides/hydroxides and increased ionization of 2,4-DCP were detrimental to the reaction (Liptak et al. 2002; Tian et al. 2009; Liu et al. 2010; Zhou et al. 2010). Furthermore, at relatively lower pH, excessive iron corrosion could occur and the produced gas of bubbles might hinder the contact of nanoparticles with the target pollutant (Zhou et al. 2010; Xiao et al. 2014), thus resulting in the decrease of removal efficiency of 2,4-DCP. From the data listed in Table 2, it could be seen distinctly that the k_{obs} increased with the increase of pH and reached to maximum when the pH value was 6. However, further increase of pH resulted in a decrease of k_{obs}.

Effect of Ni doping amount

It is generally considered that Ni doping amount is one of the significant experimental parameters affecting the removal of pollutants by iron due to hydrogenolysis requirement in the degradation process (Fang et al. 2011; Liu et al. 2013). Fixed the total loading amount of Fe and Ni, the effect of Ni doping amount on removal of 2,4-DCP was investigated, and the results were shown in Fig. 7. The 2,4-DCP removal efficiencies were 40.1%, 78.9%, 83.9%, 91.7%, 95.3%, and 86.2% within 240 min at 0%, 10%, 16%, 20%, 24%, and 30% of Ni doping amount, respectively. It was obvious that the doping of

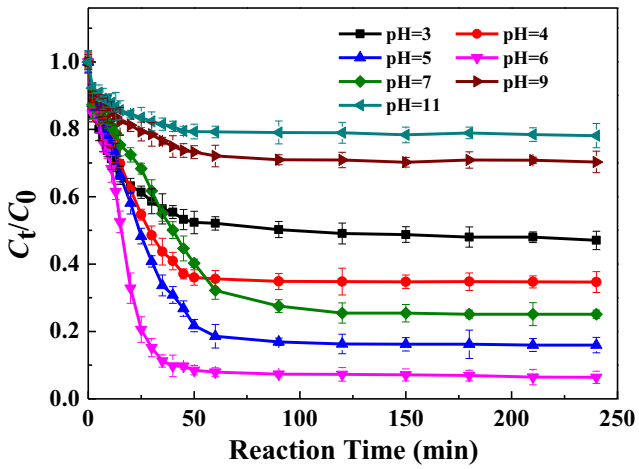

Fig. 6 Effect of solution pH on the removal of 2,4-DCP by Fe-Ni/CNTs (Conditions C_0, 300 mg/L; dosage of Fe-Ni/CNTs, 3.0 g/L; Ni doping amount, 20%; temperature, 30 °C)

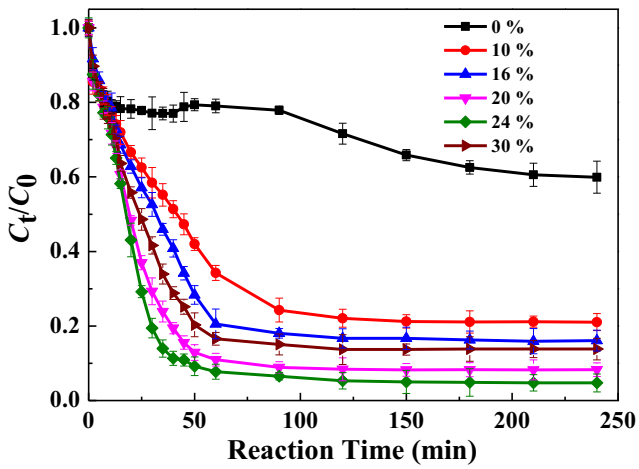

Fig. 7 Effect of Ni doping amount on the removal of 2,4-DCP (Conditions C_0, 300 mg/L; dosage of Fe-Ni/CNTs, 3.0 g/L; temperature, 30 °C)

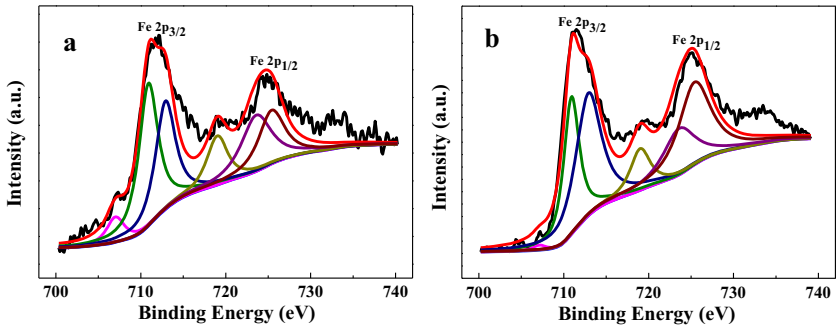

Fig. 8 XPS spectra of Fe 2p of Fe-Ni/CNTs (**a**) and Fe-Ni/CNTs-r (**b**)

Ni in Fe/CNTs greatly enhanced the removal efficiency of 2,4-DCP. The 2,4-DCP removal efficiency increased and reached to maximum with increasing the Ni doping amount to 24%. However, further enhancement of the Ni doping amount resulted in a decline of removal efficiency. The data in Table 2 showed also that the k_{obs} first showed an upward trend and then a downward one with the increase of Ni doping amount.

Promoting action of Ni in the presence of CNTs

From Fig. 3, it was evidently seen that the sample Fe-Ni/CNTs exhibited 2,4-DCP removal efficiency of about 91.7% which was highly greater than 40.1% of the sample Fe/CNTs. Previous work demonstrated that the specific surface area of material was an important factor that influenced the contaminant removal efficiency (Huang et al. 2013). However, the specific surface area could not be used for explaining the excellent 2,4-DCP removal efficiency of Fe-Ni/CNTs because it possessed a lower specific surface area compared with Fe/CNTs as mentioned above. It was just the doping of Ni in Fe that played a crucial role in promoting the catalytic removal of 2,4-DCP. It was reported that the Ni component could promote the effective dissociation of hydrogen produced by Fe corrosion into active atomic hydrogen (Lin et al. 2012; O'Carroll et al. 2013; Gao et al. 2016). In order to prove the effect of Ni in the presence of CNTs, the liquid phase catalytic hydrodechlorination of 2,4-DCP on Ni/CNTs, Fe/CNTs, and CNTs was carried out under a hydrogen atmosphere. It was found that the corresponding catalytic removal efficiency of 2,4-DCP on Ni/CNTs under hydrogen atmosphere was approximate 88.5%, which increased visibly with respect to nitrogen atmosphere. However, for Fe/CNTs and CNTs, the removal efficiencies of 2,4-DCP were no obvious differences under different atmosphere. The result implied that Ni was well served as a hydrogenation catalyst to dissociate adsorbed H_2 into active hydrogen, which could accelerate the catalytic removal of 2,4-DCP. As regards the removal efficiency of sample Fe-Ni/AC was similarly lower than that of the sample Fe-Ni/CNTs. That is to say, the same bimetallic component supported on activated carbon exhibited much lower catalytic activity although it had larger specific surface area. Therefore, we concluded that the increased catalytic activity of Fe-Ni/CNTs not only originated from the promoting action of Ni doping but also related to the property of support. It was well known that the metal species with low or zero valence could be obtained under the spontaneous redox of CNTs (Song et al. 2010). This would further facilitate the reduction of iron oxides into zero valence iron. Generally, Raman spectroscopy was used to estimate the disorder degree of CNTs and the higher I_D/I_G ratio suggested the higher extent of structure defects (Yang et al. 2013; Sun et al. 2016). As illustrated in Fig. S2, the Fe-Ni/CNTs with higher defect density exhibited larger degradation efficiency of 2,4-DCP owing to the larger electron transfer on the defective CNTs (Yang et al. 2010; Song

Table 3 Results for analyzing Fe $2p_{3/2}$ spectra of Fe-Ni/CNTs and Fe-Ni/CNTs-r after deconvolution

Sample	Assignment	Location (eV)	Percentage (%)
Fe-Ni/CNTs	Fe^0	707.0	8.5
	Fe_2O_3	710.9	51.2
	FeOOH	712.9	40.3
Fe-Ni/CNTs-r	Fe^0	707.0	1.2
	Fe_2O_3	710.9	40.2
	FeOOH	712.9	58.6

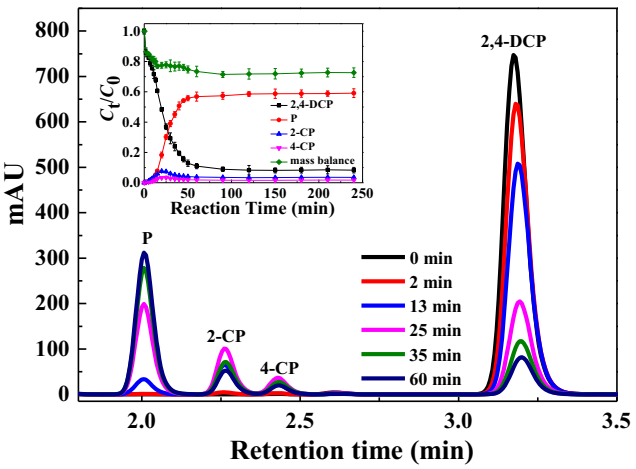

Fig. 9 HPLC chromatograms of 2,4-DCP at different reaction times (Conditions C_0, 300 mg/L; dosage of Fe-Ni/CNTs, 3.0 g/L; Ni doping amount, 20%; temperature, 30 °C)

et al. 2011), which further facilitated the formation of active hydrogen. Besides, the reduced aggregation of Fe-Ni nanoparticles promoted by CNTs as shown in Fig. 1 was also contributed to the enhancement of the catalytic activity of Fe-Ni/CNTs with respect to Fe-Ni.

To further understand the promoting action of Ni in the presence of CNTs for the catalytic removal of 2,4-DCP, we investigated the XPS spectra of Fe-Ni/CNTs before and after reaction. Fig. S3 depicted the XPS survey scan spectra of Fe-Ni/CNTs and Fe-Ni/CNTs-r, and distinct C 1 s, O 1 s, Fe 2p, and Ni 2p were observed. While the XPS spectra of Fe 2p of Fe-Ni/CNTs and Fe-Ni/CNTs-r were shown in Fig. 8. They could be split into six peaks for evaluating iron valence states. The binding energies at 710.9 and 723.6 eV for Fe $2p_{3/2}$ and Fe $2p_{1/2}$ peaks confirmed the existence of Fe_2O_3 (Wu et al. 2014). The peaks located at 712.9 and 725.4 eV indicated that FeOOH was also present on the catalyst surface (Grosvenor et al. 2004; Biesinger et al. 2011; Li et al. 2013). The characteristic peak at 707.1 eV in the Fe $2p_{3/2}$ region was ascribed to Fe^0 (Fang et al. 2011; Li et al. 2013). Moreover, a shoulder at 719.0 eV was also observed which resulted from the overlap of the shake-up satellite of oxidized iron ($2p_{3/2}$) and zero-valent iron ($2p_{1/2}$) (Bhowmick et al. 2014). Table 3 listed the results by analyzing all the Fe $2p_{3/2}$ spectra after deconvolution. As shown in Table 3, the relative atomic percentage of Fe_2O_3 in Fe-Ni/CNTs-r decreased from 51.2 to 40.2%, illustrating that the formation of FeOOH by consumption of Fe^0 and Fe_2O_3 was accompanied by the catalytic reaction process. The phenomenon inferred that the iron corrosion reaction did occur in water and led to the formation of hydrogen, which was consistent with the characterization results of XRD/EDS. Subsequently, active atomic hydrogen was generated around the Ni catalyst, which could be utilized to substitute the chlorines. Fig. S4 exhibited the XPS spectra of Ni 2p of Fe-Ni/CNTs and Fe-Ni/CNTs-r. The Ni 2p peaks at 861.5 and 880.1 eV in both samples were due to multielectron excitation (Sun et al. 2016). The Ni $2p_{3/2}$ peaks appeared at binding energies of 852.8, 854.2, 855.5, and 857.2 eV were assigned to Ni, NiO, $Ni(OH)_2$, and NiOOH species, respectively. The other peaks located at 870.1, 871.6, 873.2, and 874.5 eV in the Ni $2p_{1/2}$ region were attributed to Ni, NiO, $Ni(OH)_2$, and NiOOH species, respectively (Li et al. 1999; Velu et al. 2005; Solsona et al. 2012; Zhou et al. 2014; Sun et al. 2016). The existence of metallic Ni was convinced in Fe-Ni/CNTs and Fe-Ni/CNTs-r. The formation of $Ni(OH)_2$ was perhaps ascribed to the reaction of NiO with H_2O in an air atmosphere, and then was further oxidized to generate NiOOH. According to the relative areas of characteristic peaks, the relative atomic percentage of Ni in Fe-Ni/CNTs and Fe-Ni/CNTs-r was about 13.2% and 10.1%, respectively. It inferred that there were no significant differences of the relative contributions of Ni in the sample Fe-Ni/CNTs before and after the reaction. Therefore, it was thought that the catalytic degradation of 2,4-DCP by Fe under the stimulating of Ni changed from electron–transfer mechanism to hydrodechlorination mechanism, where Fe mainly acted as a reducing agent to produce hydrogen via iron corrosion and Ni acted as a hydrogenation catalyst to dissociate hydrogen into active atomic hydrogen. CNTs as support not only could effectively reduce the aggregation of nanoparticles but also facilitate the mass transfer of 2,4-DCP and the formation of active hydrogen. Moreover, we knew that the redox potentials for Fe^{2+}/Fe and Ni^{2+}/Ni were − 0.441 V and − 0.257 V, respectively. It indicated that the doping of Ni could also facilitate the corrosion of Fe and then accelerate the catalytic removal of 2,4-DCP. It was thereby considered that the enhanced catalytic degradation removal of Fe-Ni/CNTs for 2,4-DCP was ascribed to the synergistic effect of Fe-Ni nanoparticles and CNTs.

Analysis of dechlorination products and the possible catalytic degradation mechanism

The main dechlorination products of 2,4-DCP degradation by Fe-Ni/CNTs were identified by HPLC. As shown in Fig. 9, 2,4-DCP, 4-CP, 2-CP, and P were eluted at a relative retention time of 3.20, 2.43, 2.26, and 2.01 min, respectively. More

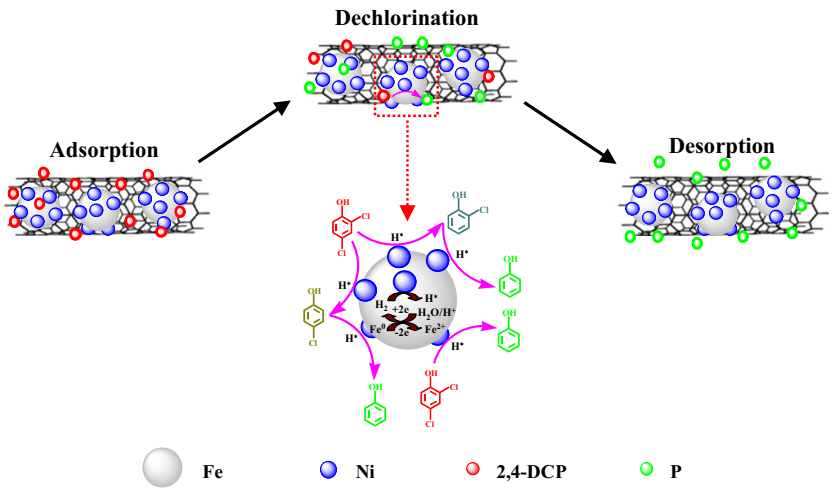

Fig. 10 Schematic diagram of catalytic degradation mechanism of 2,4-DCP by Fe-Ni/CNTs

detailed description of the chemical conversion of 2,4-DCP was displayed in the inserted figure. It was distinctly found that the amount of P continuously increased with the decrease of 2,4-DCP. Meanwhile, the amount of 2-CP and 4-CP increased promptly at the initial stage of the dechlorination reaction and then decreased steadily. The HPLC results well demonstrated that the dechlorination products of 2,4-DCP by Fe-Ni/CNTs were consisted of 2-CP, 4-CP, and P. It was worth noting that 2-CP was detected as the principal intermediate product, which perhaps was due to the difference of the Gibbs free energy of 2-CP and 4-CP (Dolfing and Harrison 1992; Xu et al. 2012). Moreover, the P formed immediately as soon as the dechlorination reaction occurred. Therefore, it was concluded that the catalytic degradation of 2,4-DCP on Fe-Ni/CNTs was a multistep reaction. Accompanied with the stepwise dechlorination, 2,4-DCP could be partly degraded directly into P. In summary, the para-Cl of 2,4-DCP was first eliminated by Fe-Ni/CNTs, then ortho-Cl, and P was the final dechlorination product.

Based on the results above, the possible catalytic degradation mechanism of 2,4-DCP by Fe-Ni/CNTs was proposed as described in Fig. 10. Firstly, the 2,4-DCP was rapidly adsorbed onto the surface of Fe-Ni/CNTs. Fe acted as a reductant to generate hydrogen gas via iron corrosion reaction in water, while Ni as a hydrogenation catalyst adsorbed H_2 and then dissociated into atomic hydrogen. In there, the produced atomic hydrogen attacked 2,4-DCP directly and led to the formation of 2-CP, 4-CP, and P through a surface-mediated process. Finally, desorption of dechlorination products into solution made the earlier 2,4-DCP occupied sites vacant and available for further adsorption and degradation of 2,4-DCP. During the catalytic degradation, the excellent adsorption-dissociation capacity of Ni for hydrogen crucially governed the process of 2,4-DCP dechlorination. The support CNTs with peculiar tubular structure not only improved the dispersion of nanoparticles but also facilitated the mass transfer of 2,4-DCP and the formation of active hydrogen. Consequently, the promoting action of Ni for Fe catalysis in the presence of CNTs remarkably enhanced the catalytic degradation performance of Fe-Ni/CNTs for 2,4-DCP.

Conclusions

In this work, Fe-Ni/CNTs were successfully prepared, characterized, and utilized for the catalytic removal of 2,4-DCP in aqueous solution. Enhanced catalytic removal performance of 2,4-DCP by Fe-Ni/CNTs was achieved, which could be ascribed to the synergistic effect between Fe-Ni nanoparticles and CNTs. The removal efficiency increased with decreasing initial concentration of 2,4-DCP and increasing dosage of Fe-Ni/CNTs. The removal of 2,4-DCP was pH-dependent and weak acidic condition was more favorable for dechlorination. The removal kinetics of 2,4-DCP by Fe-Ni/CNTs fitted well with a pseudo-first-order model. The degradation mechanism of 2,4-DCP by Fe-Ni/CNTs involved the adsorption by CNTs and catalytic reduction, where Fe acted as a reductant to generate hydrogen gas via iron corrosion and Ni as a hydrogenation catalyst promoted the dissociation of hydrogen, and a multistep dechlorination process with the preference of para-Cl > ortho-Cl.

Funding Information This work was financially supported by the National Natural Science Foundation of China (No.41877118 and 21573104), the Natural Science Foundation of Jiangsu Province of China (No.BK20181479), and the Natural Science Foundation of the Jiangsu Higher Education Institutions of China (No.17KJB610013 and 17KJA610006).

References

Bhowmick S, Chakraborty S, Mondal P, Renterghem WV, Berghe SVD, Roman Ross G, Chatterjee D, Iglesias M (2014) Montmorillonite-supported nanoscale zero-valent iron for removal of arsenic from aqueous solution: kinetics and mechanism. Chem Eng J 243:14–23

Biesinger MC, Payne BP, Grosvenor AP, Lau LWM, Gerson AR, Smart RSC (2011) Resolving surface chemical states in XPS analysis of first row transition metals, oxides, and hydroxides: Cr, Mn, Fe, Co and Ni. Appl Surf Sci 257:2717–2730

Chaudhary D, Ansari MZ, Khare N, Vankar VD (2017) Preparation, characterization and photocatalytic activity of anatase, rutile TiO_2/multiwalled carbon nanotubes nanocomposite for organic dye degradation. J Nanosci Nanotechnol 17:1894–1900

Chen QQ, Wu PX, Li YY, Zhu NW, Dang Z (2009) Heterogeneous photo-Fenton photodegradation of reactive brilliant orange X-GN over iron-pillared montmorillonite under visible irradiation. J Hazard Mater 168:901–908

Chen ZX, Jin XY, Chen ZL, Megharaj M, Naidu R (2011) Removal of methyl orange from aqueous solution using bentonite-supported nanoscale zero-valent iron. J Colloid Interf Sci 36:601–607

Cheng R, Wang JL, Zhang WX (2007) Comparison of reductive dechlorination of p-chlorophenol using Fe^0 and nanosized Fe^0. J Hazard Mater 144:334–339

Cheng R, Zhou W, Wang JL, Qi DD, Guo L, Zhang WX, Qian Y (2010) Dechlorination of pentachlorophenol using nanoscale Fe/Ni particles: role of nano-Ni and its size effect. J Hazard Mater 180:79–85

Contreras S, Rodriguez M, Al Momani F, Sans C, Esplugas S (2003) Contribution of the ozonation pre-treatment to the biodegradation of aqueous solutions of 2,4-dichlorophenol. Water Res 37:3164–3171

Dolfing J, Harrison BK (1992) Gibbs free energy of formation of halogenated aromatic compounds and their potential role as electron acceptor in anaerobic environments. Environ Sci Technol 26:2213–2216

Doong RA, Saha S, Lee CH, Lin HP (2015) Mesoporous silica supported bimetallic Pd/Fe for enhanced dechlorination of tetrachloroethylene. RSC Adv 5:90797–90805

Fang ZQ, Qiu XH, Chen JH, Qiu XQ (2011) Debromination of polybrominated diphenyl ethers by Ni/Fe bimetallic nanoparticles: influencing factors, kinetics, and mechanism. J Hazard Mater 185:958–969

Fang LP, Xu CH, Zhang WB, Huang LZ (2018) The important role of polyvinylpyrrolidone and Cu on enhancing dechlorination of 2,4-dichlorophenol by Cu/Fe nanoparticles: performance and mechanism study. Appl Surf Sci 435:55–64

Gao Y, Wang FF, Wu Y, Naidu R, Chen ZL (2016) Comparison of degradation mechanisms of microcystin-LR using nanoscale zero-valent iron (nZVI) and bimetallic Fe/Ni and Fe/Pd nanoparticles. Chem Eng J 285:459–466

Grosvenor AP, Kobe BA, Biesinger MC, Mcintyre NS (2004) Investigation of multiplet splitting of Fe 2p XPS spectra and bonding in iron compounds. Surf Interface Anal 36:1564–1574

He YH, Lin H, Dong YB, Li B, Wang L, Chu SY, Luo MK, Liu JF (2018) Zeolite supported Fe/Ni bimetallic nanoparticles for simultaneous removal of nitrate and phosphate: synergistic effect and mechanism. Chem Eng J 347:669–681

Huang Q, Liu W, Peng PA, Huang WL (2013) Reductive dechlorination of tetrachlorobisphenol A by Pd/Fe bimetallic catalysts. J Hazard Mater 262:634–641

Kanel SR, Manning B, Charlet L, Choi H (2005) Removal of arsenic(III) from groundwater by nanoscale zero-valent iron. Environ Sci Technol 39:1291–1298

Kim HS, Lee H, Han KS, Kim JH, Song MS, Park MS, Lee JY, Kang JK (2005) Hydrogen storage in Ni nanoparticle-dispersed multiwalled carbon nanotubes. J Phys Chem B 109:8983–8986

Kragulj M, Trickovic J, Kukovecz A, Jovic B, Molnar J, Roncevic S, Konya Z, Dalmacija B (2015) Adsorption of chlorinated phenols on multiwalled carbon nanotubes. RSC Adv 5:24920–24929

Li H, Li HX, Dai WL, Wang WJ, Fang ZG, Deng JF (1999) XPS studies on surface electronic characteristics of Ni-B and Ni-P amorphous alloy and its correlation to their catalytic properties. Appl Surf Sci 152:25–34

Li YM, Zhang Y, Li JF, Sheng GD, Zheng XM (2013) Enhanced reduction of chlorophenols by nanoscale zerovalent iron supported on organobentonite. Chemosphere 92:368–374

Li SP, Ma XL, Liu LJ, Cao XH (2015) Degradation of 2,4-dichlorophenol in wastewater by low temperature plasma coupled with TiO_2 photocatalysis. RSC Adv 5:1902–1909

Li H, Qiu YF, Wang XL, Yang J, Yu YJ, Chen YQ, Liu YD (2017) Biochar supported Ni/Fe bimetallic nanoparticles to remove 1,1,1-trichloroethane under various reaction conditions. Chemosphere 169:534–541

Lin YM, Chen ZL, Megharaj M, Naidu R (2012) Degradation of scarlet 4BS in aqueous solution using bimetallic Fe/Ni nanoparticles. J Colloid Interf Sci 381:30–35

Liptak MD, Gross KC, Seybold PG, Feldgus S, Shields GC (2002) Absolute pK(a) determinations for substituted phenols. J Am Chem Soc 124:6421–6427

Liu QS, Zheng T, Wang P, Jiang JP, Li N (2010) Adsorption isotherm, kinetic and mechanism studies of some substituted phenols on activated carbon fibers. Chem Eng J 157:348–356

Liu XW, Chen ZX, Chen ZL, Megharaj M, Naidu R (2013) Remediation of Direct Black G in wastewater using kaolin-supported bimetallic Fe/Ni nanoparticles. Chem Eng J 223:764–771

Liu ZT, Gu CG, Ye M, Bian YY, Cheng YW, Wang F, Yang XL, Song Y, Jiang X (2015) Debromination of polybrominated diphenyl ethers by attapulgite-supported Fe/Ni bimetallic nanoparticles: influencing factors, kinetics and mechanism. J Hazard Mater 298:328–337

Mishra A, Sharma M, Mehta A, Basu S (2017) Microwave treated bentonite clay based TiO_2 composites: an efficient photocatalyst for rapid degradation of methylene blue. J Nanosci Nanotechnol 17: 1149–1155

Nagpal V, Bokare AD, Chikate RC, Rode CV, Paknikar KM (2010) Reductive dechlorination of ϒ-hexachlorocyclohexane using Fe-Pd bimetallic nanoparticles. J Hazard Mater 175:680–687

Nasser A, Mingelgrin U (2014) Birnessite-induced mechanochemical degradation of 2,4-dichlorophenol. Chemosphere 107:175–179

O'Carroll D, Sleep B, Krol M, Boparai H, Kocur C (2013) Nanoscale zero valent iron and bimetallic particles for contaminated site remediation. Adv Water Resour 51:104–122

Pulido Melian E, Gonzalez Diaz O, Dona Rodriguez JM, Arana J, Perez Pena J (2013) Adsorption and photocatalytic degradation of 2,4-dichlorophenol in TiO_2 suspensions: effect of hydrogen peroxide, sodium peroxodisulphate, and ozone. Appl Catal A Gen 455:227–233

Sahu RS, Li DL, Doong RA (2018) Unveiling the hydrodechlorination of trichloroethylene by reduced graphene oxide supported bimetallic Fe/Ni nanoparticles. Chem Eng J 334:30–40

Shih YH, Hsu CY, Su YF (2011) Reduction of hexachlorobenzene by nanoscale zero-valent iron: kinetics, pH effect, and degradation mechanism. Sep Purif Technol 76:268–274

Solsona B, Concepcion P, Hernandez S, Demicol B, Lopez Nieto JM (2012) Oxidative dehydrogenation of ethane over NiO-CeO_2 mixed oxides catalysts. Catal Today 180:51–58

Song H, Carraway ER (2005) Reduction of chlorinated ethanes by nanosized zero-valent iron: kinetics, pathways, and effects of reaction conditions. Environ Sci Technol 39:6237–6245

Song SQ, Yang HX, Rao RC, Liu HD, Zhang AM (2010) High catalytic activity and selectivity for hydroxylation of benzene to phenol over multi-walled carbon nanotubes supported Fe_3O_4 catalyst. Appl Catal A Gen 375:265–271

Song SQ, Jiang SJ, Rao RC, Yang HX, Zhang AM (2011) Bicomponent VO_2-defects/MWCNT catalyst for hydroxylation of benzene to phenol: promoter effect of defects on catalytic performance. Appl Catal A Gen 401:215–219

Su J, Lin S, Chen ZL, Megharaj M, Naidu R (2011) Dechlorination of p-chlorophenol from aqueous solution using bentonite supported Fe/Pd nanoparticles: synthesis, characterization and kinetics. Desalination 280:167–173

Sun ZR, Wei XF, Han YB, Tong S, Hu X (2013) Complete dechlorination of 2,4-dichlorophenol in aqueous solution on palladium/polymeric pyrrole-cetyl trimethyl ammonium bromide/foam-nickel composite electrode. J Hazard Mater 244-245:287–294

Sun YF, Li CS, Zhang AM (2016) Preparation of Ni/CNTs catalyst with high reducibility and their superior catalytic performance in benzene hydrogenation. Appl Catal A Gen 522:180–187

Tian H, Li JJ, Mu Z, Li LD, Hao ZP (2009) Effect of pH on DDT degradation in aqueous solution using bimetallic Ni/Fe nanoparticles. Sep Purif Technol 66:84–89

Tsang DCW, Graham NJD, Lo IMC (2009) Humic acid aggregation in zero-valent iron systems and its effects on trichloroethylene removal. Chemosphere 75:1338–1343

Velu S, Suzuki K, Vijayaraj M, Barman S, Gopinath CS (2005) In situ XPS investigations of $Cu_{1-x}Ni_xZnAl$-mixed metal oxide catalysts used in the oxidative steam reforming of bio-ethanol. Appl Catal B Environ 55:287–299

Wei JJ, Xu XH, Liu Y, Wang DH (2006) Catalytic hydrodechlorination of 2,4-dichlorophenol over nanoscale Pd/Fe: reaction pathway and some experimental parameters. Water Res 40:348–354

Weng XL, Sun Q, Lin S, Chen ZL, Megharaj M, Naidu R (2014) Enhancement of catalytic degradation of amoxicillin in aqueous solution using clay supported bimetallic Fe/Ni nanoparticles. Chemosphere 103:80–85

Witonska IA, Walock MJ, Binczarski M, Lesiak M, Stanishevsky AV, Karski S (2014) Pd-Fe/SiO_2 and Pd-Fe/Al_2O_3 catalysts for selective hydrodechlorination of 2,4-dichlorophenol into phenol. J Mol Catal A Chem 393:248–256

Wu PX, Liu CM, Huang ZJ, Wang WM (2014) Enhanced dechlorination performance of 2,4-dichlorophenol by vermiculite supported iron nanoparticles doped with palladium. RSC Adv 4:25580–25587

Xiao JN, Yue QY, Gao BY, Sun YY, Kong JJ, Gao Y, Li Q, Wang Y (2014) Performance of activated carbon/nanoscale zero-valent iron

for removal of trihalomethanes (THMs) at infinitesimal concentration in drinking water. Chem Eng J 253:63–72

Xu J, Lv XS, Li JD, Li YY, Shen L, Zhou HY, Xu XH (2012) Simultaneous adsorption and dechlorination of 2,4-dichlorophenol by Pd/Fe nanoparticles with multi-walled carbon nanotube support. J Hazard Mater 225-226:36–45

Xu JL, Li YL, Jing C, Zhang HC, Ning Y (2014) Removal of uranium from aqueous solution using montmorillonite-supported nanoscale zero-valent iron. J Radioanal Nucl Chem 299:329–336

Yang HX, Song SQ, Rao RC, Wang XZ, Yu Q, Zhang AM (2010) Enhanced catalytic activity of benzene hydrogenation over nickel confined in carbon nanotubes. J Mol Catal A Chem 323:33–39

Yang M, Ling Q, Rao RC, Yang HX, Zhang QY, Liu HD, Zhang AM (2013) Mn_3O_4-NiO-Ni/CNTs catalysts prepared by spontaneous redox at high temperature and their superior catalytic performance in selective oxidation of benzyl alcohol. J Mol Catal A Chem 380:61–69

Zhang Z, Cissoko N, Wo JJ, Xu XH (2009) Factors influencing the dechlorination of 2,4-dichlorophenol by Ni-Fe nanoparticles in the presence of humic acid. J Hazard Mater 165:78–86

Zhang ZY, Lu M, Zhang ZZ, Xiao M, Zhang M (2012) Dechlorination of short chain chlorinated paraffins by nanoscale zero-valent iron. J Hazard Mater 243:105–111

Zhou T, Li YZ, Lim TT (2010) Catalytic hydrodechlorination of chlorophenols by Pd/Fe nanoparticles: comparisons with other bimetallic systems, kinetics and mechanism. Sep Purif Technol 76:206–214

Zhou SM, Li Y, Chen JT, Liu ZM, Wang ZH, Na P (2014) Enhanced Cr(VI) removal from aqueous solutions using Ni/Fe bimetallic nanoparticles: characterization, kinetics and mechanism. RSC Adv 4:50699–50707

Zhou ZM, Ruan WJ, Huang HH, Shen CH, Yuan BL, Huang CH (2016) Fabrication and characterization of Fe/Ni nanoparticles supported by polystyrene resin for trichloroethylene degradation. Chem Eng J 283:730–739